Nanoscale Advances

ROYAL SOCIETY OF CHEMISTRY

PAPER

View Article Online
View Journal | View Issue

Cite this: *Nanoscale Adv.*, 2022, **4**, 2180

Nitrogen-doped molecular bowls as electron donors in photoinduced electron transfer reactions†

O. A. Stasyuk, [ab] A. J. Stasyuk, *[ab] M. Solà *[a] and A. A. Voityuk *[a]

Received 10th March 2022
Accepted 27th March 2022

DOI: 10.1039/d2na00150k

rsc.li/nanoscale-advances

In recent years, the chemistry of curved π-conjugated molecules has experienced a sharp rise. The inclusion of a heteroatom in the carbon network significantly affects its semiconducting properties. In this work, we computationally study the photoinduced electron transfer in a series of C_{60} fullerene complexes with experimentally established nitrogen-doped molecular bowls. Our results demonstrate that introducing nitrogen into pentagonal rings of the bowl-shaped π-conjugated molecules and extending the π-conjugation can modulate their electron-transfer properties. Among the studied complexes, the ***hub*-NCor⊃C_{60}** complex exhibits the most desirable combination of ultrafast charge separation and slow charge recombination, suggesting its potential use in photovoltaics.

Introduction

Significant advances in the chemistry of curved π-conjugated molecules observed in the last few decades are the result of the progress in their synthesis.[1,2] The bowl-shaped compounds can be considered as structural parts of fullerenes and have attracted great attention[3] since the discovery of fullerenes[4] and nanotubes.[5] Historically, the first synthesized buckybowl with C_{5v} symmetry is corannulene (**Cor**). In 1966, Barth and Lawton reported on the multistage synthesis of dibenzo[*ghi*,*-mno*]fluoranthene called corannulene.[6] Synthesis of sumanene (**Sum**) – a fullerene segment with C_{3v} symmetry – was carried out almost 40 years later by Sakurai and Hirao (Fig. 1).[7] In the early 1990s the development of the flash vacuum pyrolysis (FVP) method enabled materials scientists to evaluate these compounds.[8–11] This attention to bowl-shaped molecules arises not only from aesthetic pleasure of curved π-conjugated systems, but also from the fact that they contribute to fundamental research of aromaticity,[12] complexation with molecules and metal ions,[13,14] and strain energy.[1,15,16] It is known that the introduction of heteroatoms into a carbon π-conjugated system can dramatically affect its properties. Doping with nitrogen or boron atoms influences the semiconducting and luminescent properties of carbon materials due to changes in the band structure.[17] Also, the introduction of the heteroatom can create "special areas" due to their electronegative or electropositive characteristics.[18] Moreover, nitrogen-embedded bowl-shaped molecules are used as model compounds for azafullerenes and nitrogen-doped nanotubes.[19–21]

There are two main types of heteroatom positions within bowl-shaped π-conjugated molecules: the *rim* position, in which a CH unit on the *rim* of a bowl is replaced by a heteroatom; and the *hub* position where a heteroatom is embedded in the central part and connects with three other atoms of the bowl. To date there have only been limited reports on the synthesis of such bowl-shaped compounds.

The first example of azabuckybowl–triazasumanene (***rim*-3NSum**) – was reported by Higashibayashi and co-workers in 2012.[20] This is the only synthesized nitrogen-doped sumanene derivative.

The synthesis of azapentabenzocorannulene bearing a nitrogen atom in the core of corannulene (***hub*-NCor**) was independently reported in 2015 by Ito and Nozaki, as well as by Hiroto and Shinokubo.[22,23] Azadibenzocorannulene with a nitrogen on the *rim* position (***rim*-NCor**) was described by Scott two years later.[24] Very recently, Krzeszewski *et al.* reported a new nitrogen-containing bowl-shaped molecule (**PP-bowl**) consisting of a pyrrolo[3,2-*b*]pyrrole core substituted with six arene rings linked in a circle.[25] In contrast to the "classical" azabuckybowls, the presented bowl features two pentagonal rings located between two heptagons. This molecule could be used as an optoelectronic material due to the electron-rich nature of the pyrrolo[3,2-*b*]pyrrole fragment.[26] Hydrazinobuckybowl, a diaza analog of diindenochrysene (**Hyd-bowl**) with a particularly electron-rich nature, was reported by Higashibayashi and co-workers.[27] More recently, the structure of the nitrogen-embedded π-extended cyclazine (**Cyc-bowl**) was described in 2020 by Deng and Zhang.[28] In general, the introduction of nitrogen or other heteroatoms into bowl-shaped π-conjugated

[a]*Institut de Química Computacional, Departament de Química, Universitat de Girona, C/ Maria Aurèlia Capmany 69, 17003 Girona, Spain. E-mail: antony.stasuk@gmail.com; miquel.sola@udg.edu; alexander.voityuk@gmail.com*

[b]*Faculty of Chemistry, University of Warsaw, Pasteura 1, 02-093 Warsaw, Poland*

† Electronic supplementary information (ESI) available. See DOI: 10.1039/d2na00150k

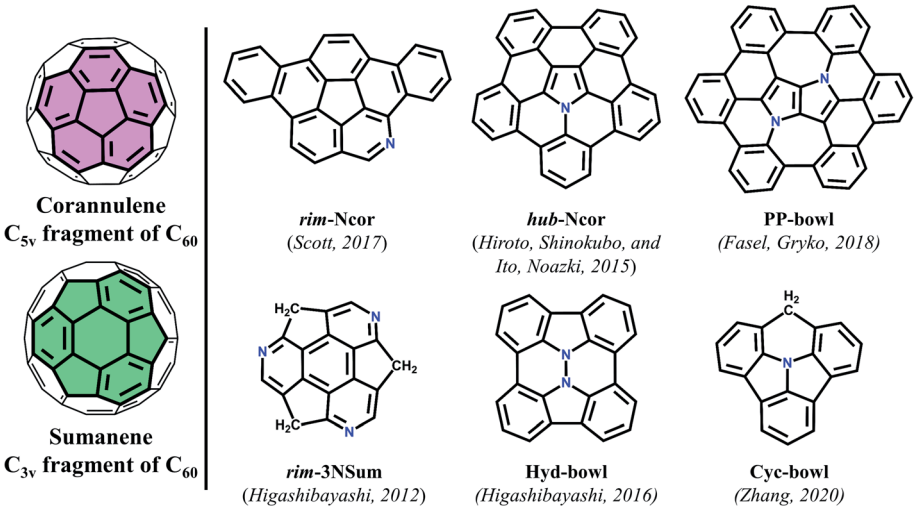

Fig. 1 Structures of nitrogen-containing molecular bowls.

molecules can be used as an effective strategy for modulating their physicochemical and electronic properties, which greatly expands the diversity and hence the use of such molecules in functional materials.

Here, we study electronic and photoinduced electron transfer (PET) properties of complexes based on C_{60} with a number of previously synthesized nitrogen-doped molecular bowls of different topologies. Using the time-dependent density functional theory (TD-DFT), we investigate the efficiency of PET in a particular complex as a function of the structural features of the bowl. The results can be used in the design of N-doped carbon nanomaterials for photovoltaic applications.

Computational methods

Geometry optimizations were performed by employing the DFT B3LYP[29–31] hybrid exchange–correlation functional with Ahlrichs' def2-SVP basis set.[32,33] The empirical dispersion D3 correction was included using the Becke–Johnson damping scheme.[34,35] Vertical excitation energies were calculated using the TDA formalism[36] with the range-separated CAM-B3LYP[37,38] functional and the def2-SVP basis set,[32,33] as implemented in the Gaussian 16 (rev. A03) program.[39] The same program was used for population analysis in terms of Mulliken,[40] Löwdin,[41] Hirshfeld,[42] iterative Hirshfeld[43] and CM5 [44] charges. The formation energy of the complexes and their strain energy were computed with the B3LYP-D3(BJ)/def2-TZVP//B3LYP-D3(BJ)/def2-SVP scheme.[45] A Morokuma-like energy decomposition analysis (EDA)[46–48] was performed using the Amsterdam Density Functional (ADF) program at the B3LYP-D3(BJ)/TZP//B3LYP-D3(BJ)/def2-SVP.[49] The topological analysis of the electron density distribution was conducted using the "Quantum Theory of Atoms in Molecules" (QTAIM).[50] The AIMALL suite of programs[51] was applied to evaluate the bond critical points and associated bond descriptors. Molecular structures and frontier molecular orbitals were visualized using the Chemcraft 1.8 program.[52] Details on the analysis of excited states, calculation of solvent effects, electron transfer rates, reorganization and interaction energies can be found in the ESI.†

Results and discussion

Ground state properties

The complementary concave–convex interaction between C_{60} fullerene and pristine corannulene leads to the formation of an 1 : 1 complex. Although the complex was observed in the gas-phase and on a metal surface, its binding constant is not high. Yokoi *et al.* found that enhanced electron donating properties of the molecular bowl cause its closer association with electron-deficient C_{60} both in solution and in the solid state. In particular, the binding constant between the *tert*-butyl derivative of ***hub*-NCor** and C_{60} was measured to be 3.8×10^3 L mol^{-1},[23] in contrast to the binding constant values of 280–475 L mol^{-1} for substituted corannulenes.[53] The pronounced electron-rich character of the nitrogen-containing bowls and the electron-deficient nature of C_{60} encouraged us to study the ground state (GS) properties of six van der Waals (vdW) complexes, ***rim*-NCor⊃C$_{60}$, *hub*-NCor⊃C$_{60}$, PP-bowl⊃C$_{60}$, Hyd-bowl⊃C$_{60}$, Cyc-bowl⊃C$_{60}$,** and ***rim*-3NSum⊃C$_{60}$** (Fig. 2), and their response to photoexcitation compared with the reference systems **Cor⊃C$_{60}$** and **Sum⊃C$_{60}$**. The selected bowls are synthesized derivatives of corannulene and sumanene with the nitrogen atom located at different positions. ***Rim*-NCor⊃C$_{60}$** and ***rim*-3NSum⊃C$_{60}$** contain pyridinic N atoms on the periphery, and **Cyc-bowl⊃C$_{60}$** has a pyramidal amine N atom, while pyrrolic N atoms are contained in the central part of other bowls. Each type of N atom has a different effect on the electronic and photophysical properties of the bowls and their complexes.

First, we consider such effects in the bowls by analyzing the frontier molecular orbitals: the highest occupied molecular orbital (HOMO) and lowest unoccupied molecular orbital (LUMO). For the bowls with pyrrolic N in a *hub* position, we found a significant reduction in the HOMO–LUMO (HL) gap compared to the undoped bowls (Fig. 2). This can be explained

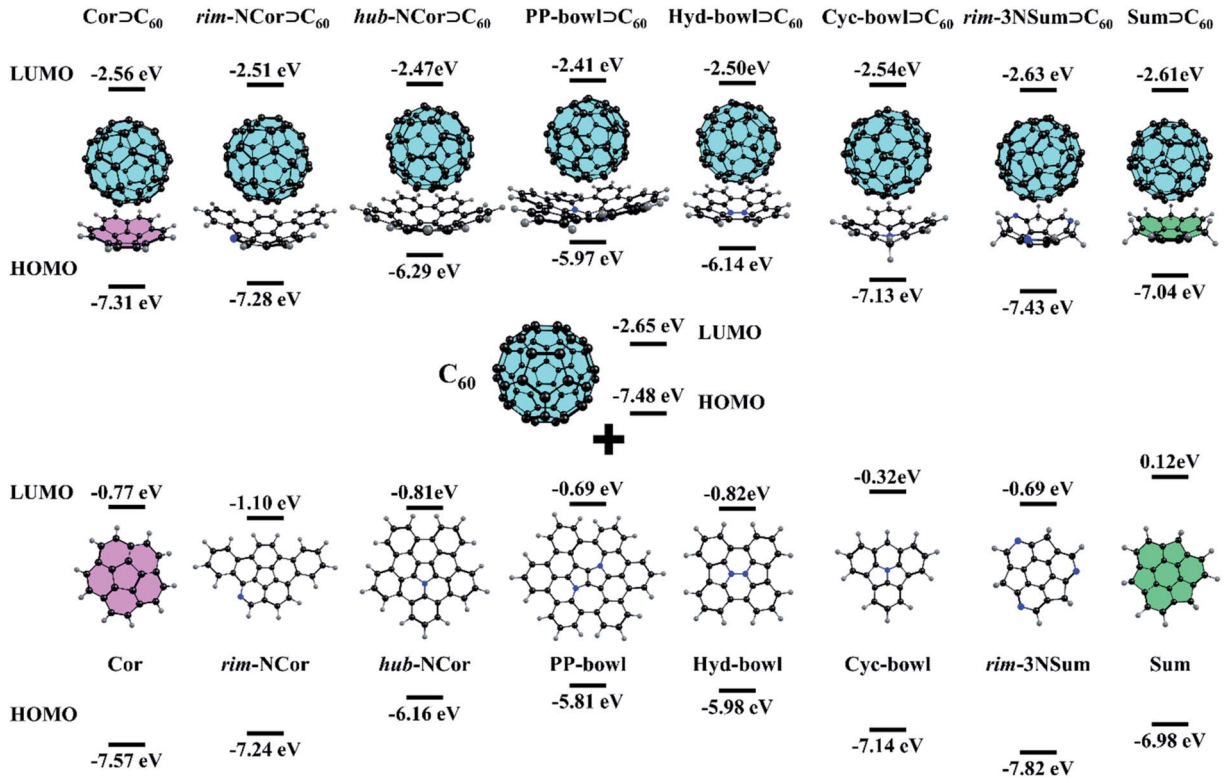

Fig. 2 Structures and HOMO/LUMO energies of the studied complexes.

by the formation of an aromatic sextet in pentagonal rings and by increasing π-electron delocalization in the bowls. The electron-donating character of the bowls can be described by the HOMO energy. The donating effects decrease by passing from the **PP-bowl** and **Hyd-bowl** with two N atoms to ***hub*-NCor** with one pyrrolic N atom. The lowest donating properties are found for ***rim*-NCor** and ***rim*-3NSum bowls** having pyridinic N.

It is important to note that the LUMO of complexes is localized on the C_{60} fragment in each case, while the localization of the HOMO depends on the complex. Because the HOMO of **Cor** and ***rim*-3NSum** bowls is lower than that of C_{60}, the HOMO of their complexes is localized on the fullerene. In other complexes, the HOMO is localized on the bowls. The HL gap (Table S1, ESI†) also depends on the complex. For example, ***hub*-NCor⊃C$_{60}$, PP-bowl⊃C$_{60}$,** and **Hyd-bowl⊃C$_{60}$** have a relatively small HL gap (3.6 to 3.8 eV), while it is about 1 eV larger (ranging from 4.4 to 4.8 eV) in ***rim*-NCor⊃C$_{60}$, *rim*-3NSum⊃C$_{60}$,** and **Cyc-bowl⊃C$_{60}$,** as well as in the reference systems **Cor⊃C$_{60}$** and **Sum⊃C$_{60}$**. Thus, the HL gap is modulated by the nitrogen content and topology of the π-conjugated system. A larger number of pyrrolic N atoms and an increase in π-conjugation promote narrowing of the HL gap. The formation of the vdW complexes has a rather small effect on the orbital energies of their fragments. In particular, the LUMO energy of the C_{60}

Table 1 Energy decomposition analysis for Cor⊃C_{60}, *rim*-NCor⊃C_{60}, *hub*-NCor⊃C_{60}, PP-bowl⊃C_{60}, Hyd-bowl⊃C_{60}, Cyc-bowl⊃C_{60}, *rim*-3NSum⊃C_{60}, and Sum⊃C_{60}[a]

		Energy components				
Complex	d^b **Bowl**⋯**C$_{60}$**	ΔE_{int}	ΔE_{Pauli}	ΔE_{elstat}	ΔE_{oi}	ΔE_{disp}
Cor⊃C$_{60}$	5.949	−18.84	35.51	−17.54 (32.3%)	−8.20 (15.1%)	−28.62 (52.6%)
***rim*-NCor⊃C$_{60}$**	5.599	−24.52	42.35	−20.42 (30.5%)	−10.00 (15.0%)	−36.45 (54.5%)
***hub*-NCor⊃C$_{60}$**	5.462	−30.79	48.41	−23.36 (29.5%)	−11.45 (14.5%)	−44.40 (56.1%)
PP-bowl⊃C$_{60}$	5.370	−33.51	49.06	−23.94 (29.0%)	−11.77 (14.3%)	−46.85 (56.7%)
Hyd-bowl⊃C$_{60}$	5.746	−24.40	40.83	−20.40 (31.3%)	−10.10 (15.5%)	−34.73 (53.2%)
Cyc-bowl⊃C$_{60}$	5.995	−18.52	34.04	−16.66 (31.7%)	−8.47 (16.1%)	−27.43 (52.2%)
***rim*-3NSum⊃C$_{60}$**	6.114	−17.98	30.37	−14.21 (29.4%)	−7.53 (15.6%)	−26.61 (55.0%)
Sum⊃C$_{60}$	5.943	−19.71	37.95	−18.25 (31.6%)	−9.29 (16.1%)	−30.13 (52.2%)

[a] The energy values are in kcal mol^{-1}. The percentage contributions to the sum of attraction energies (ΔE_{elstat} + ΔE_{oi} + ΔE_{disp}) are given in parentheses. [b] Distances between the centers of **C$_{60}$** and **Bowl** fragments are in Å.

fragment changes within only 0.25 eV compared to the isolated C_{60}, while the variation in the HOMO energy located on bowls does not exceed 0.17 eV. The population analysis does not reveal any significant charge transfer between the host (**Bowl**) and the guest (C_{60}) in the GS (Table S2, ESI†). Because of that, only minor changes are found in the HOMO and LUMO energies of the molecules by the formation of their complexes.

The stability of the complexes was evaluated by calculating the interaction energy (ΔE_{int}) between the bowls and C_{60} (see Table 1). Using a Morokuma-type energy decomposition method, the interaction energy is divided into four components: Pauli repulsion (ΔE_{Pauli}), electrostatic (ΔE_{elstat}), orbital interactions (ΔE_{oi}), and dispersion correction (ΔE_{disp}) (see computational details in the ESI†).

As seen in Table 1, the least stable complex is ***rim*-3NSum⊃C$_{60}$** due to the larger bowl-depth and weaker dispersion interactions. More extended and less curved buckybowls (***hub*-NCor** and **PP-bowl**) form the most stable complexes with C_{60}. In these complexes, there are shorter distances between the centers of C_{60} and **Bowl** fragments, more stabilizing dispersion interactions and more destabilizing Pauli repulsions. ΔE_{Pauli} varies from 30.4 kcal mol^{-1} for ***rim*-3NSum⊃C$_{60}$** to 49.1 kcal mol^{-1} for **PP-bowl⊃C$_{60}$**. Among the intermolecular attractions (electrostatic, orbital, and dispersion interactions), the last term dominates contributing from 52 to 57%. It is followed by the electrostatic (about 30%) and orbital (14 to 16%) interactions. We note that the HL gap increases with ΔE_{oi} (Fig. 2). A similar picture was found earlier in vdW complexes of C_{60} with phosphangulene oxide derivatives.[54]

The topological analysis based on Bader's atoms in molecules theory (QTAIM) was used to obtain additional information about the host–guest interactions. The electron density, its Laplacian, and other topological parameters at the bond critical points (BCPs) were calculated (see Table S3†). The analysis revealed that there are only π⋯π interactions between the host and guest units in **Cor⊃C$_{60}$**, ***rim*-NCor⊃C$_{60}$**, ***hub*-NCor⊃C$_{60}$**, **PP-bowl⊃C$_{60}$**, **Hyd-bowl⊃C$_{60}$**, and **Cyc-bowl⊃C$_{60}$**. Additional interactions of the CH⋯π type are found in ***rim*-3NSum⊃C$_{60}$** and **Sum⊃C$_{60}$**. QTAIM molecular graphs for the complexes are given in Fig. S1, ESI.† The topology of the host–guest interactions in the complexes was also described using the non-covalent interaction index (NCI).[55] The NCI isosurfaces are fairly evenly distributed between the **Bowl** and C_{60} fragments and have a similar shape in all complexes. The reduced density gradient (RDG) plots and NCI isosurfaces are presented in Fig. S2 and S3, ESI.†

Singlet excited states

The strong electron-accepting properties of fullerene and the relatively small HL gap in the complexes suggest promising PET properties of the systems. To describe the properties of excited states, all systems were divided into 2 fragments: guest (acceptor) C_{60} and host (donor) bowls. The electron density distribution was analyzed for the 100 lowest-lying excited states.

Table 2 Excitation energies (E_x, eV), main singly excited configuration (HOMO (H)–LUMO (L)) and its weight (W), oscillator strength (f), extent of charge transfer (CT, e) or localization of exciton (χ) computed for studied complexes in the gas-phase (VAC). Key parameters are bold italic type

	Supramolecular host–guest systems **Bowl⊃C$_{60}$**							
	Cor	***rim*-NCor**	***hub*-NCor**	**PP-bowl**	**Hyd-bowl**	**Cyc-bowl**	***rim*-3NSum**	**Sum**
LE$_1$ (fullerene C$_{60}$)								
Ex	***2.561***	***2.570***	***2.563***	***2.560***	***2.557***	***2.551***	***2.566***	***2.552***
Trans. (W)	H–L (0.27)	H−1–L+1 (0.22)	H−2–L+2 (0.32)	H−3–L+2 (0.20)	H−1–L (0.28)	H−2–L+1 (0.16)	H–L (0.46)	H−4–L+1 (0.21)
f	<0.001	<0.001	<0.001	<0.001	<0.001	<0.001	<0.001	<0.001
χ	0.974	0.974	0.898	0.952	0.967	0.955	0.979	0.928
LE$_2$ (Bowl)								
Ex	3.976	3.883	3.245	2.984	3.284	4.152[a]	4.171	4.143
Trans. (W)	H−6–L+6 (0.36)	H−5–L+3 (0.22)	H–L+7 (0.42)	H–L+7 (0.69)	H–L+7 (0.90)	H–L+6 (0.37)	H−5–L+6 (0.39)	H–L+6 (0.21)
f	<0.001	0.019	0.048	0.003	0.001	0.019	0.019	<0.001
χ	0.856	0.796	0.925	0.879	0.950	0.543	0.848	0.788
Most absorptive transition								
Ex	4.393	4.391	4.388	4.399	4.404	4.369	4.390	4.389[b]
Trans. (W)	H–L+5 (0.22)	H−1–L+4 (0.16)	H−3–L+4 (0.14)	H−7–L+3 (0.14)	H−5–L+3 (0.18)	H–L+5 (0.23)	H–L+3 (0.19)	H−2–L+3 (0.14)
f	0.357	0.255	0.251	0.306	0.297	0.385	0.303	0.199
Localiz.	**C$_{60}$**	**C$_{60}$**	**C$_{60}$**	**C$_{60}$**	**C$_{60}$**	**C$_{60}$**	**C$_{60}$**	**C$_{60}$**
χ	0.946	0.811	0.910	0.884	0.913	0.903	0.897	0.684
CT (Bowl → fullerene C$_{60}$)								
Ex	***3.835***	***3.413***	***2.310***	***2.078***	***2.120***	***3.214***	***3.913***	***3.137***
Trans. (W)	H−6–L (0.62)	H−5–L+2 (0.69)	H–L+1 (0.81)	H–L+1 (0.63)	H–L (0.73)	H−5–L+1 (0.49)	H−6–L+1 (0.32)	H−1–L (0.58)
f	0.002	0.003	0.008	<0.001	<0.001	<0.001	0.005	0.008
CT	0.856	0.968	0.871	0.966	0.904	0.804	0.854	0.870

[a] LE$_2$ state is partially delocalized over the C$_{60}$ unit. [b] Mixed state with significant contributions of LE and CT.

Three types of excited states were identified: (1) locally excited (LE) states, in which the excitation is mostly localized either on the guest (LE_1) or on the host molecule (LE_2) and charge transfer is less than 0.1*e* (CT < 0.1*e*); (2) charge transfer (CT) states showing a significant charge separation (CT > 0.8*e*); and (3) mixed states, where both LE and CT states contribute substantially (0.1*e* < CT < 0.8*e*).[14,56]

In the gas-phase, the 100 lowest vertical singlet excitation energies of the complexes are found in the range from 2.55 to 5.25 eV. The analysis revealed two types of LE states (LE_1 and LE_2) but only one type of CT state. This CT type corresponds to electron transfer from **Bowl** to C_{60}, leading to **Bowl**$^+\supset C_{60}^-$. CT states with opposite charge separation, **Bowl**$^-\supset C_{60}^+$, were not found in the studied energy range. We note that in all complexes the lowest LE states localized on C_{60} are dark. Thus, they can only be populated due to the fast internal conversion of absorbing states of C_{60}.

Depending on the nature of the first excited state, the complexes can be divided into two groups. The first group includes ***hub*-NCor⊃C$_{60}$**, **PP-bowl⊃C$_{60}$**, and **Hyd-bowl⊃C$_{60}$**, in which the CT state is the lowest-lying excited state with the energy ranging from 2.08 to 2.31 eV (Table 2). The second group includes **Cor⊃C$_{60}$**, ***rim*-NCor⊃C$_{60}$**, **Cyc-bowl⊃C$_{60}$**, ***rim*-3NSum⊃C$_{60}$**, and **Sum⊃C$_{60}$**. In this group, the LE_1 state with the excitation on C_{60} is the lowest one, and the energy of CT states varies from 3.14 to 3.91 eV. We note that in all complexes the energy of LE_2 states with the exciton localized on **Bowl** is higher than that of LE_1 and CT states. For each system, the excited states with a significant oscillator strength are almost completely localized on the C_{60} fragment. The selected LE and CT states were additionally analyzed in terms of natural transition orbitals (NTOs), which are shown in Fig. S4–S11 in the ESI.† The NTOs corresponding to local excitations in the C_{60} and **Bowl** fragments are of π type and rather evenly distributed over the entire fragment. The occupied and vacant NTOs associated with CT are localized on the bowls and the fullerene, respectively. The main contributions of the Kohn–Sham orbitals to the NTOs are provided in Table S4, ESI.†

Effects of the environment

A well-proven COSMO-like model[14,57–59] with dichloromethane (DCM) as a solvent was applied to estimate the effect of the polar environment on electronic excitations. The GS dipole moment of the studied complexes is in the range of 0.2 to 1.9 D. The small dipole moments can be explained by the high symmetry of the units (bowls and fullerene) and their mutual arrangement. The GS solvation energy varies from −0.15 to −0.28 eV. The reference corannulene and sumanene complexes have the lowest solvation energies. The higher solvation energy of the complexes with nitrogen-containing bowls is due to the polar C–N bonds. A change in the dipole moment ($\Delta\mu$) due to GS → LE excitations is rather small and does not exceed 3.9 D. The solvation energies of the GS, LE_1, and LE_2 states are found to be similar. Detailed solvation data including the analysis of excited states in DCM are given in Tables S5 and S6, ESI.† As expected, the dipole moment of CT states is significantly larger than that of GS and LE states. Depending on a particular complex, $\Delta\mu^{CT}$ varies from 21.4 to 26.4 D. The solvation energy of the **Bowl**$^+\supset C_{60}^-$ CT states is significantly larger. Note that the solvent stabilization of CT states in **Cor⊃C$_{60}$** and ***rim*-3NSum⊃C$_{60}$** is not strong enough to energetically enable the LE_1 →CT transition. In contrast, the stabilization of the CT state in ***rim*-NCor⊃C$_{60}$**, **Cyc-bowl⊃C$_{60}$**, and **Sum⊃C$_{60}$** is sufficient to reduce the gap between CT and LE_1 to less than 0.3 eV (Fig. 3).

Electron transfer rates and the effect of excited state geometry relaxation

CT states in the complexes are characterized by a very weak oscillator strength and can therefore not be directly populated by light absorption. However, they can be generated by the decay of LE states. Our calculations showed that excitations with the highest probability of absorption are localized on the fullerene unit. The rates of charge separation (k_{CS}) and charge recombination (k_{CR}) were calculated using the semi-classical method proposed by Ulstrup and Jortner.[60] Within this

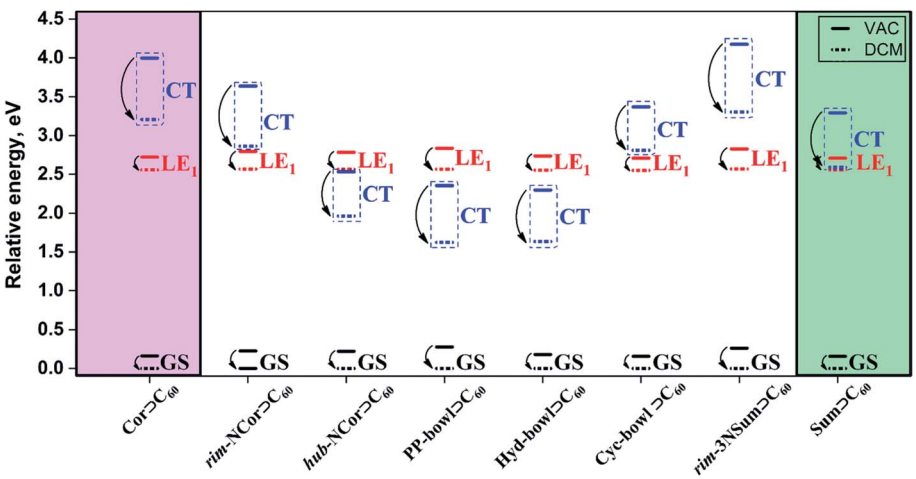

Fig. 3 Relative energies (in eV) of GS, LE_1, and CT states for the complexes of interest computed in a vacuum (VAC) and dichloromethane (DCM).

approach, the intramolecular relaxation associated with ET is described by an effective vibrational mode, and the rate is controlled by four parameters: electronic coupling of the initial and final states V_{ij}, solvation reorganization energy λ_s, reaction Gibbs energy ΔG^0, and the effective Huang–Rhys factor S_{eff}. A two-state coupling scheme was employed in all cases. The rates were estimated using the effective frequency of 1600 cm^{-1}, which corresponds to the stretching of C=C bonds. Previously, we demonstrated that the rate of charge separation for similar systems does not change significantly by varying the effective frequency from 1400 to 1800 cm^{-1}.[54] Our tests for the representative complexes **Cor⊃C$_{60}$**, **Sum⊃C$_{60}$**, and ***hub*-NCor⊃C$_{60}$** confirm the small effect of the effective frequency on the CS rate (Table S7 and Fig. S12, ESI†). The computed parameters and k_{CS} in DCM are listed in Table 3.

As seen in Table 3, the electron transfer reactions in the complexes are characterized by moderate internal reorganization energies, which range from 0.15 to 0.28 eV. The $LE_1 \rightarrow CT$ charge separation process in **Cor⊃C$_{60}$** and ***rim*-3NSum⊃C$_{60}$** is unlikely because of its highly positive Gibbs energy. In turn, the modest activation energy barrier is responsible for the rather slow charge separation in ***rim*-NCor⊃C$_{60}$**, **Cyc-bowl⊃C$_{60}$**, and **Sum⊃C$_{60}$**. Electron transfer in these complexes occurs in the normal Marcus regime ($|\Delta G^0| < \lambda$) on the nanosecond timescale or even slower. The characteristic time (τ) was found to be 151.94, 2.46, and 1.07 ns, respectively. At the same time, PET in ***hub*-NCor⊃C$_{60}$**, **PP-bowl⊃C$_{60}$**, and **Hyd-bowl⊃C$_{60}$** is almost barrierless. The calculated rate constants unambiguously confirm the ultrafast charge separation between the **C$_{60}$** and **Bowl** fragments. Thus, the complexes with the bowls containing

Table 3 Charge separation rates k_{CS} (in s^{-1}), Gibbs energy ΔG^0 (in eV), electronic coupling V_{ij} (in eV), solvent (λ_s) and internal (λ_i) reorganization energy (in eV), Huang–Rhys factor (S_{eff}) and activation energy barrier (ΔE_a, eV) for Cor⊃C$_{60}$, *rim*-NCor⊃C$_{60}$, *hub*-NCor⊃C$_{60}$, PP-bowl⊃C$_{60}$, Hyd-bowl⊃C$_{60}$, Cyc-bowl⊃C$_{60}$, *rim*-3NSum⊃C$_{60}$, and Sum⊃C$_{60}$ complexes computed in DCM

			Reorg. energy, eV				
Complex	ΔG^{0a}, eV	$\lvert V_{ij}\rvert$, eV	λ_i	λ_s	$S_{eff}{}^b$	$\Delta E_a{}^c$, eV	k_{CS}, s^{-1}
Cor⊃C$_{60}$	0.652	9.35×10^{-3}	0.170	0.413	0.857	0.686	5.67×10^{0}
***rim*-NCor⊃C$_{60}$**	0.296	4.93×10^{-3}	0.151	0.338	0.761	0.297	6.63×10^{6}
***hub*-NCor⊃C$_{60}$**	−0.598	1.98×10^{-3}	0.165	0.246	0.832	0.017	3.89×10^{12}
PP-bowl⊃C$_{60}$	−0.942	2.22×10^{-3}	0.250	0.322	1.260	0.016	2.29×10^{10}
Hyd-bowl⊃C$_{60}$	−0.918	2.20×10^{-3}	0.277	0.345	1.396	0.015	3.16×10^{10}
Cyc-bowl⊃C$_{60}$	0.260	1.91×10^{-2}	0.218	0.312	1.099	0.262	4.06×10^{8}
***rim*-3NSum⊃C$_{60}$**	0.736	1.17×10^{-2}	0.212	0.407	1.069	0.802	9.82×10^{-2}
Sum⊃C$_{60}$	0.034	1.96×10^{-3}	0.166	0.410	0.836	0.120	9.39×10^{8}

[a] Gibbs energy difference between CT and LE_1 states. [b] Effective value of the Huang–Rhys factor $S_{eff} = \lambda_i/\hbar\omega_{eff}$, where $\hbar\omega_{eff}$ is set to 1600 cm^{-1}. [c] Activation energy barrier for the $LE_1 \rightarrow CT$ reaction.

Table 4 Charge recombination rates k_{CR} (in s^{-1}), Gibbs energy ΔG^0 (in eV), electronic coupling V_{ij} (in eV), solvent (λ_s) and internal (λ_i) reorganization energy (in eV), Huang–Rhys factor (S_{eff}) and activation energy barrier (ΔE_a, eV) for *rim*-NCor⊃C$_{60}$, *hub*-NCor⊃C$_{60}$, PP-bowl⊃C$_{60}$, Hyd-bowl⊃C$_{60}$, Cyc-bowl⊃C$_{60}$, and Sum⊃C$_{60}$ complexes computed in vertical and relaxed geometries in DCM

			Reorg. energy, eV				
Complex	ΔG^{0a}, eV	$\lvert V_{ij}\rvert$, eV	λ_i	λ_s	$S_{eff}{}^b$	$\Delta E_a{}^c$, eV	k_{CR}, s^{-1}
Vertical Frank–Condon geometries							
***rim*-NCor⊃C$_{60}$**	−2.863	6.62×10^{-2}	0.140	0.338	0.706	0.058	2.46×10^{3}
***hub*-NCor⊃C$_{60}$**	−1.965	4.10×10^{-2}	0.145	0.246	0.731	0.036	3.98×10^{7}
PP-bowl⊃C$_{60}$	−1.623	4.22×10^{-2}	0.147	0.322	0.741	0.036	7.22×10^{9}
Hyd-bowl⊃C$_{60}$	−1.635	3.44×10^{-3}	0.183	0.345	0.923	0.033	1.64×10^{8}
Cyc-bowl⊃C$_{60}$	−2.590	7.40×10^{-2}	0.164	0.312	0.827	0.047	3.96×10^{5}
Sum⊃C$_{60}$	−3.304	1.22×10^{-2}	0.165	0.410	0.832	0.066	4.28×10^{0}
Relaxed in CT geometries							
***rim*-NCor⊃C$_{60}$**	−2.614	5.82×10^{-2}	0.138	0.328	0.696	0.054	4.49×10^{4}
***hub*-NCor⊃C$_{60}$**	−1.548	2.31×10^{-2}	0.130	0.350	0.655	0.039	3.98×10^{9}
PP-bowl⊃C$_{60}$	−1.262	1.09×10^{-2}	0.136	0.326	0.686	0.030	1.39×10^{10}
Hyd-bowl⊃C$_{60}$	−0.956	3.46×10^{-2}	0.218	0.415	1.099	0.017	6.91×10^{12}
Cyc-bowl⊃C$_{60}$	−2.252	3.89×10^{-2}	0.240	0.321	1.210	0.035	1.74×10^{8}
Sum⊃C$_{60}$	−2.877	6.47×10^{-2}	0.167	0.337	0.842	0.053	1.27×10^{4}

[a] Gibbs energy difference between CT and GS. [b] Effective value of the Huang–Rhys factor $S_{eff} = \lambda_i/\hbar\omega_{eff}$, where $\hbar\omega_{eff}$ is set to 1600 cm^{-1}. [c] Activation energy barrier for the $CT \rightarrow GS$ reaction.

Table 5 Back ET rate (CT → LE_1) $k_{BET}^{LE_1}$ (in s^{-1}), Gibbs energy ΔG^0 (in eV), electronic coupling V_{ij} (in eV), solvent (λ_s) and internal (λ_i) reorganization energy (in eV), Huang–Rhys factor (S_{eff}) and activation energy barrier (ΔE_a, eV) for the ***rim*-NCor⊃C60**, **Cyc-bowl⊃C60**, and **Sum⊃C60** complexes computed in DCM

			Reorg. energy, eV				
Complex	ΔG^{0a}, eV	$\lvert V_{ij}\rvert$, eV	λ_i	λ_s	S_{eff} [b]	ΔE_a [c], eV	$k_{BET}^{LE_1}$, s^{-1}
***rim*-NCor⊃C60**	−0.296	4.93×10^{-3}	0.151	0.338	0.761	0.004	7.15×10^{12}
Cyc-bowl⊃C60	−0.260	1.91×10^{-2}	0.218	0.312	1.099	0.005	1.06×10^{13}
Sum⊃C60	−0.034	1.96×10^{-3}	0.166	0.410	0.836	0.087	3.53×10^{9}

[a] Gibbs energy difference between LE_1 and CT states. [b] Effective value of the Huang–Rhys factor $S_{eff} = \lambda_i/\hbar\omega_{eff}$, where $\hbar\omega_{eff}$ is set to 1600 cm^{-1}. [c] Activation energy barrier for the CT → LE_1 reaction.

the pyrrolic nitrogen atoms and extended π-conjugation demonstrate better PET properties.

Usually, the generated CT states are deactivated by charge recombination to the ground state. For large conjugated systems, the effect of internal geometry reorganization on ΔG^0 is rather small and can be safely neglected.[61,62] However, in the studied complexes, the **Bowl** fragment is relatively small, and the relaxation effect can be significant. Thus, we studied the effect of geometry relaxation on the rate of charge recombination in DCM for ***rim*-NCor⊃C60**, ***hub*-NCor⊃C60**, **PP-bowl⊃C60**, **Hyd-bowl⊃C60**, **Cyc-bowl⊃C60**, and **Sum⊃C60** (Table 4). The **Cor** and ***rim*-3NSum** based complexes were not considered because the formation of CT states is unlikely for them.

In contrast to the charge separation, the charge recombination reactions take place in the inverted Marcus region ($|\Delta G_0| > \lambda$). Thus, the relaxation of the CT geometry leads to a decrease in the $|\Delta G_0|$ and accordingly increases k_{CR}. Moreover, the geometry relaxation reduces the activation barrier of the CT → GS reaction.

Since the electron transfer in the ***rim*-NCor⊃C60**, **Cyc-bowl⊃C60**, and **Sum⊃C60** complexes is characterized by $\Delta G^0 > 0$ (Table 3), the charge recombination CT → LE_1 state can be considered as an alternative deactivation channel of the CT state. As seen in Table 5, the back electron transfer from the CT to the LE_1 state in the ***rim*-NCor⊃C60**, **Cyc-bowl⊃C60**, and **Sum⊃C60** complexes is rather fast. Thus, we infer that the CT states in these complexes can hardly be observed.

In summary, for **PP-bowl⊃C60**, **Hyd-bowl⊃C60**, **Cyc-bowl⊃C60**, ***rim*-NCor⊃C60**, **Cyc-bowl⊃C60**, and **Sum⊃C60** complexes, k_{CR} was found to be similar to or even higher than the corresponding charge separation rates. Fast charge recombination is a significant disadvantage as it prevents the efficient extraction of electrons and holes and, consequently, the potential application of these complexes in photovoltaic devices. Only ***hub*-NCor⊃C60** demonstrates ultrafast photoinduced electron transfer on the picosecond timescale ($\tau = 0.25$ ps) and slow charge recombination (k_{CR} is smaller by 3 orders of magnitude than k_{CS}).

Conclusions

In this work, we studied in detail the ground and excited-state properties of several complexes formed by C_{60} fullerene and nitrogen-doped molecular bowls of different topologies using the DFT/TD-DFT approach. The propensity of a particular complex to photoinduced electron transfer is mainly determined by the electron-donating properties of the bowl. The low HOMO energy of the ***rim*-3NSum** bowl results in a high activation barrier for electron transfer in ***rim*-3NSum⊃C60**, and thus inhibits this process. PET in the ***rim*-NCor⊃C60** and **Cyc-bowl⊃C60** complexes occurs in the normal Marcus regime on the nanosecond timescale. In turn, the ***hub*-NCor⊃C60**, **PP-bowl⊃C60**, and **Hyd-bowl⊃C60** complexes reveal ultrafast PET occurring on the picosecond timescale. However, the practical application of **PP-bowl⊃C60**, **Hyd-bowl⊃C60**, and **Cyc-bowl⊃C60** may be limited due to fast charge recombination. Only the ***hub*-NCor⊃C60** complex demonstrates the desirable combination of ultrafast charge separation ($\tau = 0.25$ ps) and relatively slow charge recombination. This makes it a promising candidate for applications in organic photovoltaics.

Author contributions

O. A. S.: investigation, formal analysis, writing – original draft, writing – review & editing. A. J. S.: investigation, formal analysis, writing – original draft, writing – review & editing. M. S.: supervision, writing – review & editing, funding acquisition. A. A. V.: supervision, writing – review & editing.

Conflicts of interest

There are no conflicts to declare.

Acknowledgements

We are grateful for financial support from the Spanish MINECO (Network RED2018-102815-T, project PID2020-113711GB-I00, and Juan de la Cierva contract IJC2019-039846-I to A. J. S.), the Catalan DIUE (2017SGR39), and the University of Girona (POSTDOC-UdG 2021/31 to O. A. S.). This research was supported in part by PLGrid Infrastructure.

References

1 S. H. Pun and Q. Miao, *Acc. Chem. Res.*, 2018, **51**, 1630–1642.
2 J. M. Fernández-García, P. J. Evans, S. Filippone, M. Á. Herranz and N. Martín, *Acc. Chem. Res.*, 2019, **52**, 1565–1574.

3 M. Saito, H. Shinokubo and H. Sakurai, *Mater. Chem. Front.*, 2018, **2**, 635–661.
4 H. W. Kroto, J. R. Heath, S. C. O'Brien, R. F. Curl and R. E. Smalley, *Nature*, 1985, **318**, 162–163.
5 S. Iijima, *Nature*, 1991, **354**, 56–58.
6 W. E. Barth and R. G. Lawton, *J. Am. Chem. Soc.*, 1966, **88**, 380–381.
7 H. Sakurai, T. Daiko and T. Hirao, *Science*, 2003, **301**, 1878.
8 A. Borchardt, A. Fuchicello, K. V. Kilway, K. K. Baldridge and J. S. Siegel, *J. Am. Chem. Soc.*, 1992, **114**, 1921–1923.
9 L. T. Scott, M. M. Hashemi and M. S. Bratcher, *J. Am. Chem. Soc.*, 1992, **114**, 1920–1921.
10 L. T. Scott, M. M. Hashemi, D. T. Meyer and H. B. Warren, *J. Am. Chem. Soc.*, 1991, **113**, 7082–7084.
11 G. Zimmermann, U. Nuechter, S. Hagen and M. Nuechter, *Tetrahedron Lett.*, 1994, **35**, 4747–4750.
12 S. Escayola, A. Poater, A. Muñoz-Castro and M. Solà, *Chem. Commun.*, 2021, **57**, 3087–3090.
13 S. N. Spisak, Z. Zhou, S. Liu, Q. Xu, Z. Wei, K. Kato, Y. Segawa, K. Itami, A. Y. Rogachev and M. A. Petrukhina, *Angew. Chem., Int. Ed.*, 2021, **60**, 25445–25453.
14 S. Zank, J. M. Fernández-García, A. J. Stasyuk, A. A. Voityuk, M. Krug, M. Solà, D. M. Guldi and N. Martín, *Angew. Chem., Int. Ed.*, 2022, **61**, e202112834.
15 A. S. Filatov, A. V. Zabula, S. N. Spisak, A. Y. Rogachev and M. A. Petrukhina, *Angew. Chem., Int. Ed.*, 2014, **53**, 140–145.
16 C. Liu, Y. Ni, X. Lu, G. Li and J. Wu, *Acc. Chem. Res.*, 2019, **52**, 2309–2321.
17 O. Stephan, P. M. Ajayan, C. Colliex, P. Redlich, J. M. Lambert, P. Bernier and P. Lefin, *Science*, 1994, **266**, 1683–1685.
18 S. Hiroto, *Chem. Lett.*, 2021, **50**, 1146–1155.
19 S. Maldonado, S. Morin and K. J. Stevenson, *Carbon*, 2006, **44**, 1429–1437.
20 Q. Tan, S. Higashibayashi, S. Karanjit and H. Sakurai, *Nat. Commun.*, 2012, **3**, 891.
21 K. Gong, F. Du, Z. Xia, M. Durstock and L. Dai, *Science*, 2009, **323**, 760–764.
22 S. Ito, Y. Tokimaru and K. Nozaki, *Angew. Chem., Int. Ed.*, 2015, **54**, 7256–7260.
23 H. Yokoi, Y. Hiraoka, S. Hiroto, D. Sakamaki, S. Seki and H. Shinokubo, *Nat. Commun.*, 2015, **6**, 8215.
24 V. M. Tsefrikas, A. K. Greene and L. T. Scott, *Org. Chem. Front.*, 2017, **4**, 688–698.
25 S. Mishra, M. Krzeszewski, C. A. Pignedoli, P. Ruffieux, R. Fasel and D. T. Gryko, *Nat. Commun.*, 2018, **9**, 1714.
26 M. Krzeszewski, Ł. Dobrzycki, A. L. Sobolewski, M. K. Cyrański and D. T. Gryko, *Angew. Chem., Int. Ed.*, 2021, **60**, 14998–15005.
27 S. Higashibayashi, P. Pandit, R. Haruki, S.-i. Adachi and R. Kumai, *Angew. Chem., Int. Ed.*, 2016, **55**, 10830–10834.
28 N. Deng and G. Zhang, *Org. Lett.*, 2019, **21**, 5248–5251.
29 A. D. Becke, *Phys. Rev. A: At., Mol., Opt. Phys.*, 1988, **38**, 3098–3100.
30 C. Lee, W. Yang and R. G. Parr, *Phys. Rev. B: Condens. Matter Mater. Phys.*, 1988, **37**, 785–789.
31 L. W. S. H. Vosko and M. Nusair, *Can. J. Phys.*, 1980, **58**, 1200–1211.
32 F. Weigend and R. Ahlrichs, *Phys. Chem. Chem. Phys.*, 2005, **7**, 3297–3305.
33 F. Weigend, *Phys. Chem. Chem. Phys.*, 2006, **8**, 1057–1065.
34 S. Grimme, J. Antony, S. Ehrlich and H. Krieg, *J. Chem. Phys.*, 2010, **132**, 154104.
35 S. Grimme, S. Ehrlich and L. Goerigk, *J. Comput. Chem.*, 2011, **32**, 1456–1465.
36 S. Hirata and M. Head-Gordon, *Chem. Phys. Lett.*, 1999, **314**, 291–299.
37 T. Yanai, D. P. Tew and N. C. Handy, *Chem. Phys. Lett.*, 2004, **393**, 51–57.
38 P. Besalú-Sala, A. A. Voityuk, J. M. Luis and M. Solà, *Phys. Chem. Chem. Phys.*, 2021, **23**, 5376–5384.
39 M. J. Frisch, G. W. Trucks, H. B. Schlegel, G. E. Scuseria, M. A. Robb, J. R. Cheeseman, G. Scalmani, V. Barone, G. A. Petersson, H. Nakatsuji, X. Li, M. Caricato, A. V. Marenich, J. Bloino, B. G. Janesko, R. Gomperts, B. Mennucci, H. P. Hratchian, J. V. Ortiz, A. F. Izmaylov, J. L. Sonnenberg, D. Williams-Young, F. Ding, F. Lipparini, F. Egidi, J. Goings, B. Peng, A. Petrone, T. Henderson, D. Ranasinghe, V. G. Zakrzewski, J. Gao, N. Rega, G. Zheng, W. Liang, M. Hada, M. Ehara, K. Toyota, R. Fukuda, J. Hasegawa, M. Ishida, T. Nakajima, Y. Honda, O. Kitao, H. Nakai, T. Vreven, K. Throssell, J. A. Montgomery, Jr, J. E. Peralta, F. Ogliaro, M. J. Bearpark, J. J. Heyd, E. N. Brothers, K. N. Kudin, V. N. Staroverov, T. A. Keith, R. Kobayashi, J. Normand, K. Raghavachari, A. P. Rendell, J. C. Burant, S. S. Iyengar, J. Tomasi, M. Cossi, J. M. Millam, M. Klene, C. Adamo, R. Cammi, J. W. Ochterski, R. L. Martin, K. Morokuma, O. Farkas, J. B. Foresman, and D. J. Fox, *Gaussian 16*, Revision A.03, Gaussian, Inc., Wallingford CT, 2016.
40 R. S. Mulliken, *J. Chem. Phys.*, 1955, **23**, 1833–1840.
41 P. O. Löwdin, *J. Chem. Phys.*, 1950, **18**, 365–375.
42 F. L. Hirshfeld, *Theor. Chim. Acta*, 1977, **44**, 129–138.
43 P. Bultinck, C. V. Alsenoy, P. W. Ayers and R. Carbó-Dorca, *J. Chem. Phys.*, 2007, **126**, 144111.
44 A. V. Marenich, S. V. Jerome, C. J. Cramer and D. G. Truhlar, *J. Chem. Theory Comput.*, 2012, **8**, 527–541.
45 F. Weigend, M. Häser, H. Patzelt and R. Ahlrichs, *Chem. Phys. Lett.*, 1998, **294**, 143–152.
46 K. Morokuma, *Acc. Chem. Res.*, 1977, **10**, 294–300.
47 T. Ziegler and A. Rauk, *Theor. Chim. Acta*, 1977, **46**, 1–10.
48 G. Frenking and F. M. Bickelhaupt, The EDA Perspective of Chemical Bonding, in *The Chemical Bond*, ed. G. Frenking and S. Shaik, Wiley, Weinheim, 2014, pp. 121–157.
49 ADF 2018, SCM, *Theoretical Chemistry*, Vrije Universiteit, Amsterdam, The Netherlands, http://www.scm.com.
50 R. F. W. Bader, *Chem. Rev.*, 1991, **91**, 893–928.
51 T. A. Keith, *AIMAll, Version 14.06.21*, TK Gristmill Software, Overland Park, KS, 2014.
52 G. A. Zhurko, *Chemcraft 1.80 (build 523b) – graphical program for visualization of quantum chemistry computations*, https://chemcraftprog.com.

53 S. Mizyed, P. E. Georghiou, M. Bancu, B. Cuadra, A. K. Rai, P. Cheng and L. T. Scott, *J. Am. Chem. Soc.*, 2001, **123**, 12770–12774.
54 A. J. Stasyuk, O. A. Stasyuk, M. Solà and A. A. Voityuk, *Dalton Trans.*, 2021, **50**, 16214–16222.
55 E. R. Johnson, S. Keinan, P. Mori-Sánchez, J. Contreras-García, A. J. Cohen and W. Yang, *J. Am. Chem. Soc.*, 2010, **132**, 6498–6506.
56 M. Izquierdo, B. Platzer, A. J. Stasyuk, O. A. Stasyuk, A. A. Voityuk, S. Cuesta, M. Solà, D. M. Guldi and N. Martin, *Angew. Chem., Int. Ed.*, 2019, **131**, 7006–7011.
57 A. Klamt, *J. Phys. Chem.*, 1996, **100**, 3349–3353.
58 A. J. Stasyuk, O. A. Stasyuk, M. Solà and A. A. Voityuk, *Chem.–Eur. J.*, 2019, **25**, 2577–2585.
59 O. A. Stasyuk, A. J. Stasyuk, M. Solà and A. A. Voityuk, *Phys. Chem. Chem. Phys.*, 2021, **23**, 2126–2133.
60 J. Ulstrup and J. Jortner, *J. Chem. Phys.*, 1975, **63**, 4358–4368.
61 A. J. Stasyuk, O. A. Stasyuk, M. Solà and A. A. Voityuk, *Chem. Commun.*, 2020, **56**, 12624–12627.
62 A. J. Stasyuk, O. A. Stasyuk, M. Solà and A. A. Voityuk, *J. Mater. Chem. C*, 2021, **9**, 9436–9445.